TÉCNICO LISBOA

PIC1 - Scientific Project

Analysis of Higgs Couplings and Beyond Standard Model Effects at Future e^+e^- Colliders

João Faustino

ist1106560

Supervisors:
Prof. Patricia Conde Muíño,

Prof. Inês Ochoa

June 27, 2025

Abstract

The precise measurement of Higgs boson couplings remains a central objective in high-energy physics, offering a unique window into possible extensions of the Standard Model (SM). In this study, we investigate Higgs production at future lepton colliders, focusing on the Future Circular Collider (FCC-ee) and the International Linear Collider (ILC). Using Monte Carlo simulations performed with `MadGraph5_aMC@NLO`, we analyse the processes $e^+e^- \to \nu\bar{\nu}H$ and $e^+e^- \to ZH$, with $H \to b\bar{b}$, at energies ranging from 250 to 1000 GeV. Distributions of key kinematic observables—pseudorapidity (η), transverse momentum (p_T), total momentum (p), and angular correlations ($\Delta\eta$, $\Delta\phi$) are studied in detail. We further explore the effects of a dimension-six CP-even operator from the Standard Model Effective Field Theory (SMEFT), c_{HW}, on the $\nu\bar{\nu}H$ channel at $\sqrt{s} = 300$ and 1000 GeV. The operator induces clear, percent-level deviations in the differential distributions. Our results highlight the strong sensitivity of future electron–positron colliders to deviations from the SM, and emphasise their potential to probe Higgs couplings with sub-percent precision, thereby providing a promising avenue for uncovering new physics in the electroweak sector.

I. INTRODUCTION

Currently, the prevailing theory through which we interpret the microscopic world around us is the Standard Model of particle physics (SM). This model describes the majority of interactions observed in nature, explaining the fundamental structure of matter by identifying the elementary particles, quarks and leptons, and their interactions via the four fundamental forces: the strong force, the weak force, the electromagnetic force, and gravity. The Standard Model remains, to this day, the most successful description of the subatomic world [1]. However, it presents significant limitations and fails to provide complete explanations for several observed phenomena. Among the most notable are the matter–antimatter asymmetry in the universe and the existence of dark matter and dark energy. Understanding these phenomena requires the development of theories that extend beyond the Standard Model and which often predict the existence of new particles, including potential new Higgs bosons, or variations in the properties of already known particles. Testing such theories and deepening our understanding of the universe necessitates ever more precise measurements of both known and yet-undiscovered particles [2].

Since its observation by the ATLAS and CMS collaborations in 2012, the Higgs boson has become the focal point of experimental investigations into the mechanism of electroweak symmetry breaking. Precise characterisation of its couplings to other Standard Model particles is essential both for verifying the model's internal consistency and for uncovering possible signs of new physics. Although the forthcoming High-Luminosity upgrade of the LHC (HL-LHC) promises substantial gains in statistical power, projections indicate that several Higgs couplings, particularly those to gauge bosons and third-generation fermions, will remain constrained to uncertainties of order 2–4%. Such residual imprecision limits our ability to detect small, yet theoretically motivated, deviations from Standard Model predictions. Consequently, there is a compelling case for purpose-built, high-energy electron–positron colliders. Their clean experimental environment and well-defined initial state allow coupling measurements to be performed with relative uncertainties below 0.1%, thereby opening a precision frontier capable of revealing subtle anomalies in Higgs interactions that could herald physics beyond the Standard Model[3].

In this context, the present work contributes to the effort of evaluating the potential of future accelerators — specifically the Future Circular Collider (FCC-ee) and the International Linear Collider (ILC), in probing interactions beyond the Standard Model. To this end, simulations were performed based on the projected operational parameters of both accelerators, with the aim of comparing the achievable sensitivity in each scenario and assessing their relative capabilities in studying modifications to Higgs boson couplings.

II. THE STANDARD MODEL OF PARTICLE PHYSICS

The Standard Model of Particle Physics is, to date, the most successful theory describing the fundamental constituents of matter and the forces governing their interactions, with the exception of gravity. Developed throughout the second half of the 20$^{\text{th}}$ century, this framework combines the principles of quantum mechanics with special relativity to explain phenomena at the subatomic scale. Elementary particles are organised into well-defined categories: fermions (quarks and leptons), which constitute matter, and bosons, which mediate the fundamental interactions. The model accurately accounts for three of the four known fundamental forces of nature: the electromagnetic, weak, and strong interactions [1, 3].

The theoretical foundation of the Standard Model lies in gauge symmetries, which structure the interactions as exchanges of mediator bosons. The relevant gauge groups are $U(1)$ for electromagnetism, $SU(2)$ for the weak interaction, and $SU(3)$ for the strong interaction. The unification of electromagnetism and the weak force into the electroweak theory is formalised through the symmetry group $SU(2) \times U(1)$, which predicts the existence of the $W^{\pm}$ and Z^0 bosons, as well as the Higgs field, all experimentally confirmed [4].

Fundamental particles are classified into two major families: fermions and bosons. Fermions, which have spin-1/2, are the building blocks of matter and are subdivided into quarks and leptons. Quarks carry fractional electric charge and participate in all fundamental interactions, including the strong force. There are six distinct quark flavours: up (u), down (d), charm (c), strange (s), top (t), and bottom (b), each with a corresponding antiquark 1. Leptons include the electron (e), muon (μ), tau (τ), and their associated neutrinos (ν_e, ν_μ, ν_τ) 1. These particles interact via the electromagnetic and weak forces, with the exception of neutrinos, which are electrically neutral and interact solely through the weak interaction [4].

Bosons, in turn, mediate the fundamental forces. The photon (γ) is the quantum of the electromagnetic force, massless and electrically neutral. The $W^{\pm}$ and Z^0 bosons mediate

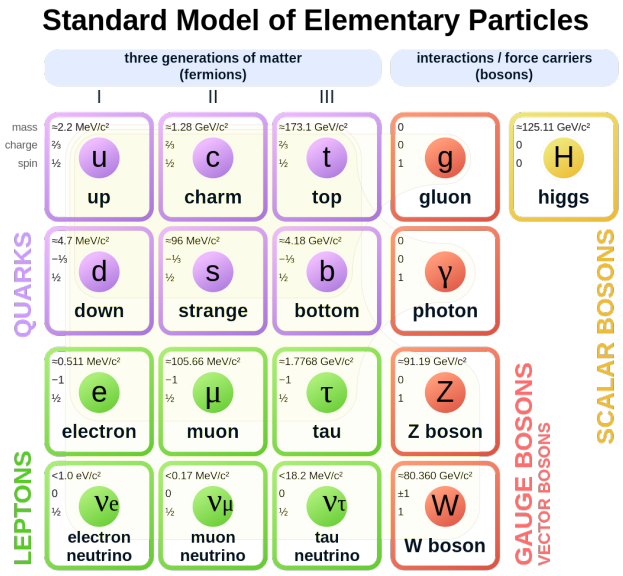

Figure 1: Representation of the Standard Model particles [4]

the weak interaction and are essential in processes such as beta decay; the W boson can carry positive or negative electric charge, while the Z boson is neutral. Gluons (g) are the carriers of the strong force, which acts between quarks and is governed by the colour dynamics of Quantum Chromodynamics (QCD). Finally, the Higgs boson (H), a spin-0 scalar particle, emerges from the Higgs mechanism and is responsible for endowing massive elementary particles with mass through spontaneous electroweak symmetry breaking [4].

A. The Higgs boson

Among the bosons mediating the fundamental interactions, as discussed in the previous section, the Higgs boson stands out for not being associated with a force in the traditional sense, but rather as the quantum manifestation of an omnipresent scalar field — the so-called Higgs field. The inclusion of this field in the Standard Model provides a gauge-invariant framework to describe the origin of mass for elementary particles through a mechanism known as *spontaneous electroweak symmetry breaking*. This section explores the formalism of the Higgs field, the structure of its potential, and the experimental implications of its discovery.

The potential associated with the Higgs field exhibits a characteristic shape often referred to as a "Mexican hat" potential as we can see from the Figure 2:

$$V(\phi) = \mu^2 \phi^\dagger \phi + \lambda (\phi^\dagger \phi)^2, \tag{1}$$

where ϕ denotes the Higgs field, μ^2 is a negative parameter, and λ is a positive constant. This potential features a non-trivial energy minimum, implying that the vacuum expectation value of the field is non-zero. Such a vacuum configuration leads to the spontaneous breaking of electroweak symmetry and enables certain particles to acquire mass proportionally to the strength of their interaction with the field.[4]

The Higgs boson is the quantum excitation of the Higgs field, corresponding to a scalar particle with spin zero. Its

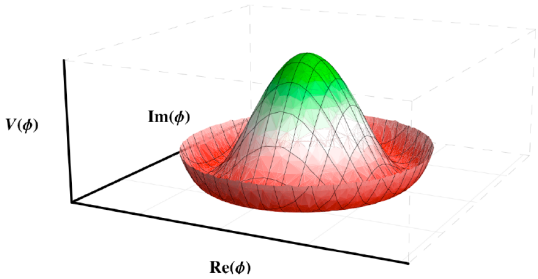

Figure 2: Higgs Potential [4]

lack of intrinsic angular momentum distinguishes it from all other known fundamental particles and is consistent with spacetime symmetry requirements. Unlike other fields, such as the electromagnetic field which depends on specific sources, the Higgs field permeates all of space, even in the absence of matter, and is essential for the structure and stability of the universe.

Experimental validation of the Higgs mechanism was achieved through the detection of the Higgs boson in high-energy collisions at the LHC. Its production occurs predominantly via gluon fusion through a loop involving top quarks. One of the most distinctive decay channels is $H \to ZZ \to 4\ell$, where the Higgs decays into two Z bosons, each subsequently decaying into a pair of charged leptons. These final-state particles allow the presence of the Higgs boson to be inferred indirectly but unambiguously [2].

To determine the Higgs couplings to different particles with greater precision, it is crucial to study multiple production and decay channels. These include processes involving real top quarks, as well as decays into heavy fermions such as bottom quarks and tau leptons. The experimental observation of these channels in recent years has confirmed the role of the Higgs mechanism in providing mass to the entire third generation of charged fermions.

To date, the couplings of the Higgs boson to vector bosons ($W^\pm$, Z^0) and third-generation fermions have been measured with precisions ranging from 5% to 20%, in good agreement with Standard Model predictions. Investigating all these interactions is one of the main motivations for developing future high-luminosity and high-precision accelerators, since the Standard Model is incomplete and exploring such processes may offer insights into possible beyond the Standard Model scenarios [2].

These experimental advances not only reinforce the Standard Model as the most complete theoretical framework currently available for describing the subatomic world, but also open the door to new physics through potential deviations in Higgs properties or the discovery of previously undetected particles.

III. OBJECTIVES AND MOTIVATION

Despite the great success of the Standard Model, several fundamental questions remain unresolved. This theory does not incorporate gravity, nor does it provide a satisfactory explanation for dark matter or dark energy, and it also fails to

clarify the origin of the observed matter-antimatter asymmetry in the universe. Moreover, the couplings of the Higgs boson to light particles, such as the electron or first-generation quarks, are extremely weak and have not yet been conclusively measured directly. These limitations motivate the development of new particle accelerators and the formulation of theories beyond the Standard Model, capable of unifying all fundamental forces and addressing current cosmological observations.

The discovery of the Higgs boson at the LHC in 2012 represented the final major experimental confirmation of the Standard Model of Particle Physics. However, it remains unclear whether the observed Higgs sector is the only one or merely part of a larger structure. In particular, the precise determination of the Higgs boson couplings to the massive vector bosons, notably the $W^{\pm}$, is essential to test the internal consistency of the model and to detect potential contributions from new physics scenarios, which could manifest as small deviations from the expected values.

The possibility of such deviations has motivated the systematic study of higher-dimensional effective operators within the framework of Effective Field Theory (EFT), which parametrizes generic effects of new physics at high energies. The observation or exclusion of anomalous terms in HWW couplings could provide crucial insights into the electroweak symmetry structure or reveal the influence of yet unknown sectors, such as additional fields, extra dimensions or strongly coupled particles [2, 5].

In this context, the present work aims to evaluate the sensitivity of future electron-positron colliders, focusing on the Future Circular Collider (FCC-ee) which cannot go beyond the energy of 350 GeV and the International Linear Collider (ILC) which in turn can go up to 1000 GeV, to the detection of interactions between the Higgs boson and other relevant particles, such as the W and Z bosons. To this end, simulated events will be generated for the following processes (see Fig.3):

$$e^+e^- \to \nu\bar{\nu}H, \quad e^+e^- \to ZH, \quad \text{and} \quad e^+e^- \to \nu\bar{\nu}H \to \nu\bar{\nu}b\bar{b}.$$

These events are produced using the `MadGraph5_aMC@NLO` event generator for various energies: 250 GeV, 300 GeV, 500 GeV, and 1000 GeV [6, 7].

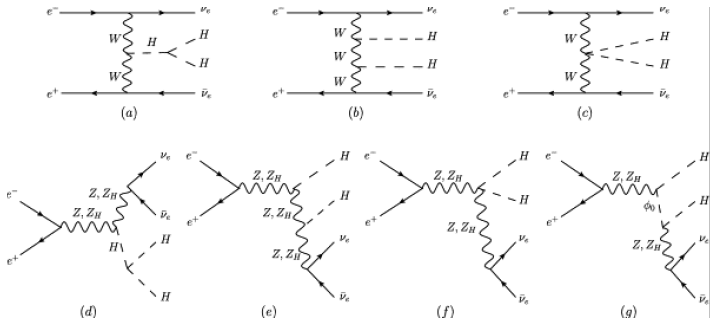

Figure 3: Feynman diagrams for Higgs production via different channels in e^+e^- colliders [8].

The data analysis will be performed using Python scripts designed to extract relevant kinematic distributions, such as pseudorapidity, transverse momentum, and the magnitude of the momentum of neutrinos and the Higgs boson. Differential variables, including $\Delta\eta$ and $\Delta\phi$ between particle pairs, will also be studied with the aim of identifying potential deviations from the Standard Model predictions. The results will be presented in normalised histograms, allowing assessment of the impact of effective operators across different energy regimes.

Building upon this analysis, the study will investigate the sensitivity of these observables to modifications induced by higher-dimensional operators. Particular emphasis is placed on the effects of the CP-even coupling c_{HW} and $c_{H\widetilde{W}}$, whose presence may subtly distort momentum distributions and angular correlations in the final state. By systematically examining these variations, the work aims to assess the potential to distinguish between such beyond Standard Model interactions in e^+e^- collisions at different energies, by identifying observables with high discriminating power. These findings lay the groundwork for future precision studies of the Higgs sector at next-generation lepton colliders, highlighting their ability to probe beyond Standard Model effects with unprecedented sensitivity.

IV. THE FUTURE CIRCULAR COLLIDER (FCC)

The Future Circular Collider (FCC) is a CERN-led initiative to develop a next-generation particle accelerator with energies and luminosities surpassing those of current facilities such as the LHC. Its aim is to extend the exploration of the Standard Model and to probe potential new physics through access to higher energy regimes [9, 10]. The proposed infrastructure consists of a circular tunnel approximately 100 km in circumference 4, significantly exceeding the LHC's 27 km, and will accommodate both electron-positron and proton-proton collisions at unprecedented scales.

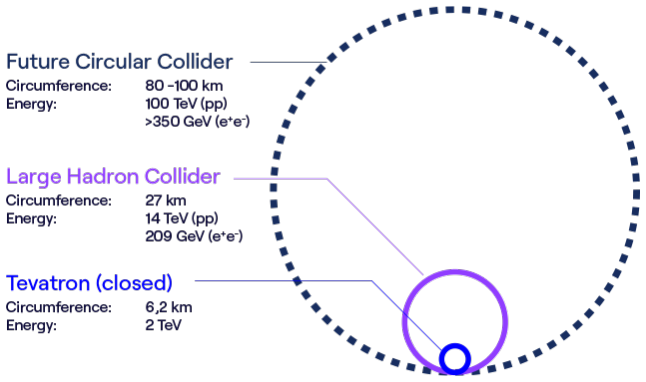

Figure 4: Comparison of tunnel sizes: FCC (100 km), LHC (27 km) and Tevatron (6 km) [9].

The FCC programme is divided into phases, initially comprising FCC-ee and FCC-hh. FCC-ee will be a high-luminosity electron-positron collider targeting precision measurements of the Higgs boson, vector bosons W and Z, and heavy quarks, enabling rigorous tests of the Standard Model and the search

for deviations indicative of new physics [10, 11]. FCC-hh will be a proton-proton collider operating at around 100 TeV, facilitating the production of heavy particles and the investigation of phenomena beyond the LHC's reach. Together, these phases offer a complementary strategy that combines precision with energy.

From a physics standpoint, the FCC will allow in-depth studies of electroweak symmetry breaking and the Higgs sector through highly precise measurements of couplings and properties. It will also test quantum chromodynamics at high energies and probe rare or suppressed Standard Model processes. The enhanced energy and luminosity will facilitate searches for phenomena predicted by theories beyond the Standard Model, including supersymmetry, extra dimensions, and potential dark matter signatures [10].

The FCC represents a major technological and collaborative endeavour, with international contributions including those from the Laboratory of Instrumentation and Experimental Particle Physics (LIP) in Portugal [12]. Despite significant engineering and experimental challenges, the project fosters advances in both scientific knowledge and technological innovation with broad applications.

V. THE INTERNATIONAL LINEAR COLLIDER (ILC)

The International Linear Collider (ILC) is a proposed linear electron-positron collider based on superconducting radiofrequency (SRF) technology. In its first stage, it is designed to operate at a energy of $\sqrt{s} = 250$ GeV, serving as a Higgs factory with upgrade potential up to 1 TeV. With polarised beams and high luminosity, the ILC would enable precision measurements of Higgs boson properties and electroweak processes, as well as sensitivity to physics beyond the Standard Model [13].

The technical design of the accelerator is mature and has benefited from international collaboration. Although a host site is yet to be confirmed, efforts continue through coordinated global R&D. The ILC Technology Network (ITN), led by KEK and involving laboratories across Europe and Asia, advances key components such as SRF cavity production, positron source development, and nano-beam stability.

These developments maintain the ILC's readiness for a potential future construction phase. Its linear design, clean collision environment, and precise beam control make it particularly suited for detailed studies of fundamental interactions at the energy frontier.

VI. COORDINATE SYSTEM

The analysis of the simulated events was performed using the coordinate system employed by the ATLAS experiment, which is similar to a right-handed reference frame with its origin at the interaction point (IP) at the centre of the detector. The z-axis is aligned with the beam direction, the x-axis points from the IP towards the centre of the LHC ring, and the y-axis points vertically upwards. In the transverse plane, cylindrical coordinates (r, ϕ) are used, where ϕ is the azimuthal angle around the z-axis. The pseudorapidity η is defined as a function of the polar angle θ by $\eta = -\ln\tan(\theta/2)$, providing a more convenient description of angular distributions at high energies.

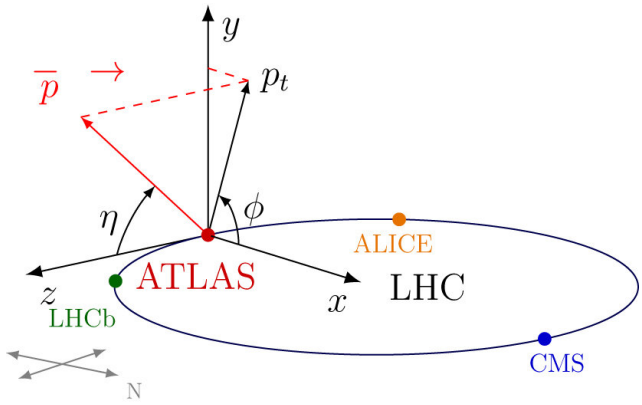

Figure 5: Coordinate system used by the ATLAS experiment.

VII. ANALYSIS OF RESULTS

A. First simulations and distributions

As an initial step in this study I began by simulating two processes. The first consists of a collision between a positron and an electron which, via the exchange of W bosons, produce a neutrino, a antineutrino, and a Higgs boson. The second process, similar to the first, also involves a collision between a positron and an electron, but results in the production of a Z boson and a Higgs boson. It is considered a relevant background when studying the $\nu\bar{\nu}H$ final state due to similar kinematic signatures (see Fig. 6).

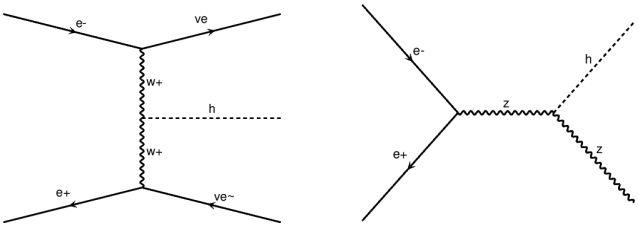

Figure 6: Schematic representation of the simulated processes: $e^+e^- \to \nu\bar{\nu}H$ (left) and $e^+e^- \to ZH$ (right).

Simulations were performed for both processes under study, considering four different energies values: 250, 300, 500, and 1000 GeV. For each of this energys, graphical representations were produced for the distributions of pseudorapidity (η), transverse momentum (p_T), and the magnitude of total momentum (p) of the most relevant particles: neutrinos and the Higgs boson.

Let us begin by analysing the pseudorapidity (η) distribution for the process $e^+e^- \to \nu\bar{\nu}H$ visible in Fig.7.

The pseudorapidity distribution for the neutrinos presents a symmetric double-peaked structure, with prominent maxima in both the positive and negative η regions. This characteristic arises because the histogram includes both the neutrino and antineutrino in a single plot. As these particles

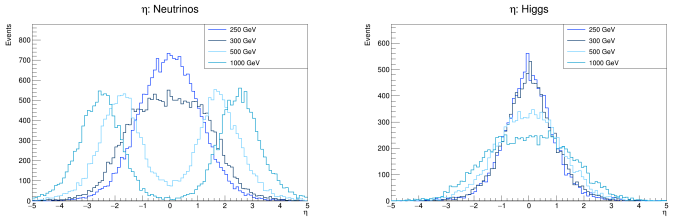

Figure 7: Pseudorapidity distributions of neutrinos (left) and Higgs boson (right) for the process $e^+e^- \to \nu\bar{\nu}H$.

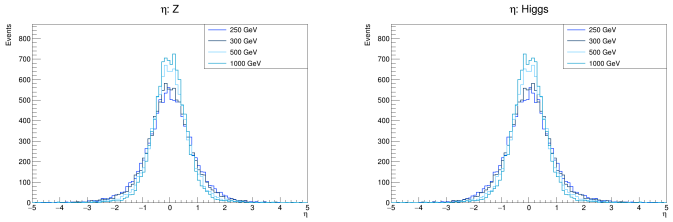

Figure 9: Pseudorapidity distributions of Z boson (left) and Higgs boson (right) for the process $e^+e^- \to ZH$.

are emitted in opposite directions, one peak corresponds to the neutrino and the other to the antineutrino. The symmetry around $\eta = 0$ reflects the initial conditions of the e^+e^- collider, which are symmetric in the centre-of-mass frame.

As the energy increases from 250 to 1000 GeV, the distribution becomes progressively wider, indicating a broader angular dispersion of the neutrinos. This is consistent with the expectation that higher-energy collisions yield products with greater longitudinal boosts, causing the neutrinos to be emitted closer to the beam direction, i.e., at higher absolute values of η.

This effect becomes more evident in figure 8, which shows simulations of the process at several intermediate energies.

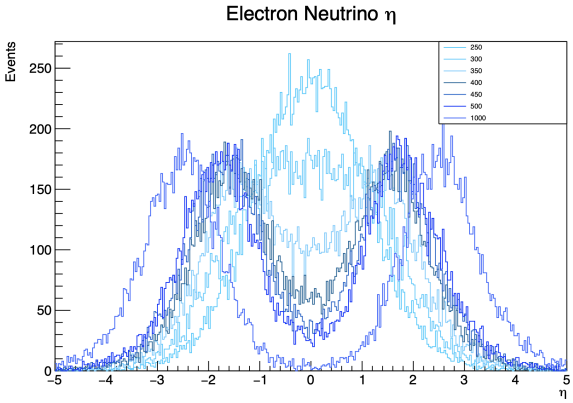

Figure 8: Pseudorapidity distributions of neutrinos with additional simulations at $\sqrt{s} = 350$, 400, and 450 GeV to illustrate the intermediate evolution between 250 and 1000 GeV.

In contrast, the pseudorapidity distribution of the Higgs boson is narrower and more centralised around $\eta = 0$. This indicates that the Higgs boson is predominantly emitted in directions perpendicular to the beam axis. Even as the collision energy increases, the peak of the distribution remains centred, although a slight broadening is observed. This suggests that the Higgs kinematics are less sensitive to boosts along the beam direction.

Now turning to the pseudorapidity distributions of the process $e^+e^- \to ZH$ shown in figure 9 the pseudorapidity distributions of the Z boson and the Higgs boson exhibit very similar shapes, displaying a mirror symmetry about $\eta = 0$. Furthermore, as the energy increases, the peaks become more pronounced while remaining centred at $\eta = 0$, without shifting towards larger absolute pseudorapidity values.

When comparing the two processes, a key distinction emerges in the structure of the pseudorapidity distributions. In the $\nu\bar{\nu}H$ case, the double-peaked shape originates from the inclusion of both neutrino and antineutrino in a single distribution, each emitted in opposite directions and contributing symmetrically about $\eta = 0$. The presence of two invisible particles allows for more varied momentum configurations, leading to broader and more dispersed distributions as the energy increases.

In contrast, the ZH process exhibits a more constrained and symmetric behaviour. Due to the two-body final state, the Z and Higgs bosons are emitted back-to-back in the centre-of-mass frame, resulting in sharply peaked and mirrored pseudorapidity distributions around $\eta = 0$. As the energy increases, the peaks become more pronounced but remain centred, reflecting the fixed angular correlation imposed by two-body kinematics.

These contrasting behaviours highlight how the number and visibility of final-state particles shape the overall pseudorapidity profiles and provide insight into the underlying event topology.

The analysis now turns to the transverse momentum (p_T) distributions depict in figure 10, which offer deeper insight into the kinematic behaviour of the final-state particles in the two processes under investigation.

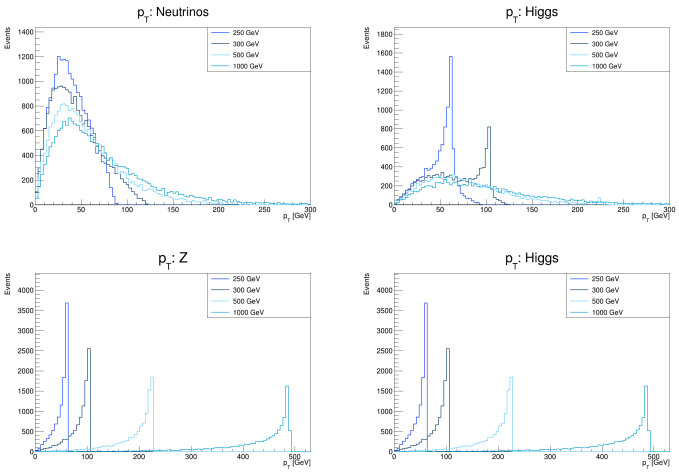

Figure 10: Transverse Momentum (p_T) distributions for the two under study processes. Top row: neutrinos (left) and Higgs boson (right) for the process $e^+e^- \to \nu\bar{\nu}H$. Bottom row: Z boson (left) and Higgs boson (right) for the process $e^+e^- \to ZH$.

Looking at the first distribution in figure 10 we can see the p_T spectra for neutrinos exhibit a clear dependence on the energy. At $\sqrt{s} = 250$ GeV, the distribution is largely con-

centrated below 100 GeV. As the collision energy increases, a noticeable extension of the tail towards higher transverse momenta is observed, with significant contributions beyond 150 GeV at $\sqrt{s} = 1000$ GeV. This trend is consistent with conservation of momentum: higher-energy collisions impart greater kinetic energy to the neutrinos, especially due to the recoil against the Higgs boson.

The broad shape of the distribution reflects the wide range of possible emission angles and kinematic configurations of the undetected neutrinos. This information is crucial for experimental searches that rely on missing transverse energy, as neutrinos escape detection and contribute significantly to the missing p_T signal.

Now turning our attention to Higgs boson's in the $e^+e^- \to \nu\bar{\nu}H$ process we can see that in contrast with the neutrinos distribution, the Higgs boson's transverse momentum is more sharply peaked and exhibits a more abrupt drop. The peak position shifts to higher p_T values with increasing $\sqrt{s}$, typically ranging from around 50 GeV to over 150 GeV. This behaviour is expected given the Higgs boson's recoil against the neutrino pair, and reflects both the mass of the Higgs and the dynamics of the production mechanism. The comparatively narrower shape also suggests a more constrained kinematic configuration.

In the $e^+e^- \to ZH$ process, both the Z and Higgs bosons display transverse momentum distributions with a single prominent peak and a roughly symmetric shape around it. As in the previous process, increasing the energy $\sqrt{s}$ leads to a shift of the spectra towards higher p_T values. At $\sqrt{s} = 250$ GeV, the transverse momenta are mostly confined below 100 GeV, whereas at $\sqrt{s} = 1000$ GeV, the distributions extend well beyond 300 GeV.

Finally, the analysis focuses on the total momentum (p) distributions depict in figure 11, providing additional insight into the kinematic properties of the final-state particles.

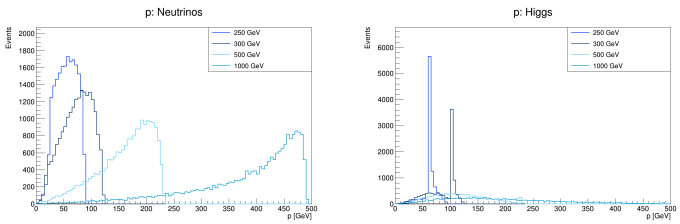

Figure 11: Total momentum (p) distributions for the process $e^+e^- \to \nu\bar{\nu}H$. The left plot shows the distribution for the neutrinos, and the right plot corresponds to the Higgs boson.

The total momentum spectrum of the neutrinos in the process $e^+e^- \to \nu\bar{\nu}H$ spans a broad range, with a long tail extending to high values as the energy $\sqrt{s}$ increases. At $\sqrt{s} = 1000$ GeV, the distribution reaches beyond 400 GeV, reflecting the significant boost these weakly interacting particles receive in energetic collisions. The distribution is asymmetric and skewed to the right, owing to the inclusion of both the neutrino and antineutrino, as well as the recoil dynamics in events with missing energy all of this visible in figure 11.

In turn the Higgs boson's in $e^+e^- \to \nu\bar{\nu}H$ process total momentum spectrum is more localised, with a peak that shifts moderately with increasing $\sqrt{s}$. Unlike the neutrino distribution, the Higgs spectrum is more symmetric and narrower, indicating a more constrained momentum range. This is consistent with its larger mass and the fact that the Higgs recoils against the neutrino pair, leading to a more predictable momentum configuration.

In the process $e^+e^- \to ZH$, the total momentum spectra of the Z and Higgs bosons consist of sharp, well-defined peaks whose positions vary with the energy. As $\sqrt{s}$ increases, the peaks shift discretely to higher momentum values, reflecting the kinematics of a two-body final state in which both particles recoil against each other. No broadening or asymmetry is observed, as each energy corresponds to a unique kinematic configuration. This behaviour is expected in idealised simulations without detector effects, and highlights the role of total momentum as a clean observable for studying the dynamics of Higgs production in electron–positron collisions.

Across all cases, the total momentum distributions follow the same general trend observed for the transverse momentum: higher collision energies yield harder spectra, with larger mean and maximum values. The shapes are typically skewed, particularly at high $\sqrt{s}$, indicating that a fraction of events involve final-state bosons carrying a substantial share of the total energy—often associated with specific recoil geometries and low-momentum emission of accompanying particles.

These results offer a comprehensive view of how different final-state configurations affect the kinematic profiles of Higgs and associated particles in e^+e^- collisions.

B. Simulating Higgs Decay into $b\bar{b}$

Building on the previous analysis, we then simulated the process $e^+e^- \to \nu\bar{\nu}H$ but now explicitly considering the decay of the Higgs boson into a $b\bar{b}$ pair.

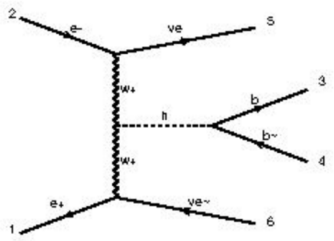

Figure 12: Schematic representation of the simulated processe: $e^+e^- \to \nu\bar{\nu}H$ with $b\bar{b}$ pair decay.

This simulation allowed us to analyse the kinematic distribution of the b-jets and compare their properties with those of the previously studied particles, in particular, the changes introduced in the distributions of pseudorapidity, transverse momentum, and total momentum.

When analysing the particles previously studied, specifically the neutrinos and the Higgs boson, we found that their pseudorapidity, transverse momentum, and total momentum distributions remained largely unchanged.

In addition to the distributions of the previously studied particles (neutrinos and Higgs boson, now considering its decay), the simulation now provides access to the pseudorapidity, transverse momentum, and total momentum distribu-

tions for the Higgs decay products: the b and $\bar{b}$ quarks. Let us begin by examining the pseudorapidity distributions of the decay products 13.

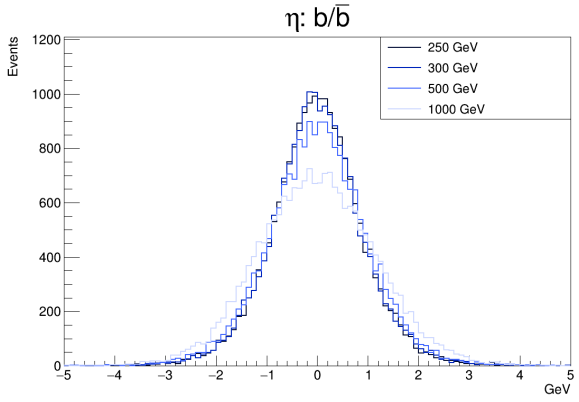

Figure 13: Pseudorapidity distribution of the b and $\bar{b}$ quarks resulting from the Higgs boson decay in the process $e^+e^- \to \nu\bar{\nu}H$.

This distribution of the b and $\bar{b}$ quarks, visible in the figure 13, exhibits a profile centred around $\eta = 0$, with a relatively narrow width compared to the neutrino distributions. This central concentration indicates that the b-jets are predominantly emitted in directions transverse to the beam axis, which is consistent with a Higgs boson produced with low longitudinal momentum in the laboratory frame. As the energy increases, the η distribution becomes slightly broader, reflecting the boost imparted to the Higgs system, although the b-jets remain largely centralised due to the decay kinematics of a scalar particle.

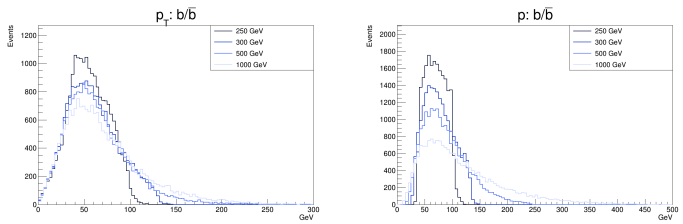

Figure 14: Transverse momentum (left) and total momentum (right) distributions of the b and $\bar{b}$ quarks resulting from the Higgs boson decay in the process $e^+e^- \to \nu\bar{\nu}H$.

Regarding the total momentum (p) and transverse momentum (p_T) distributions showed in figure 14, a clear energy dependence is observed. Both distributions exhibit a peak that shifts towards higher values with increasing $\sqrt{s}$, consistent with the growing energy available to the system. The shape of the p distribution indicates a relatively broad momentum spectrum, while the p_T distribution displays a pronounced peak that gradually flattens as the energy increases. This behaviour reflects the expected kinematics of the Higgs decay into two mass particles and confirms the successful reconstruction of the b-jets' kinematic properties from the simulated events.

C. Analysis of Angular Correlations: $\Delta\eta$ and $\Delta\phi$ Distributions

In addition to the kinematic properties of individual particles, an essential part of the analysis involves studying angular correlations between the final-state particles. These correlations, quantified through the pseudorapidity separation ($\Delta\eta$) and azimuthal angle separation ($\Delta\phi$), provide insight into the spatial configuration of the events and are directly related to the underlying physics processes. This study focuses on the process $e^+e^- \to \nu\bar{\nu}H$, with the Higgs boson decaying into a $b\bar{b}$ pair.

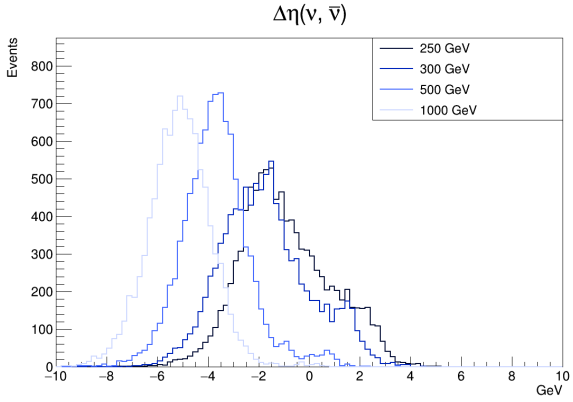

Figure 15: difference in pseudorapidity between the neutrino and the antineutrino.

Looking first at the $\Delta\eta$ between the neutrino and the antineutrino represented in figure 15, we observe that the shape of the distributions is asymmetric and significantly shifted towards negative values, with the peak moving from approximately -2 to around -6 as the energy increases. Unlike distributions centered at zero, this behavior is expected in this case: the neutrino is predominantly emitted in the direction of the incoming electron, while the antineutrino follows the direction of the incoming positron. This reflects the underlying topology of the process, in which each lepton radiates a W boson that subsequently fuses to produce the Higgs boson.

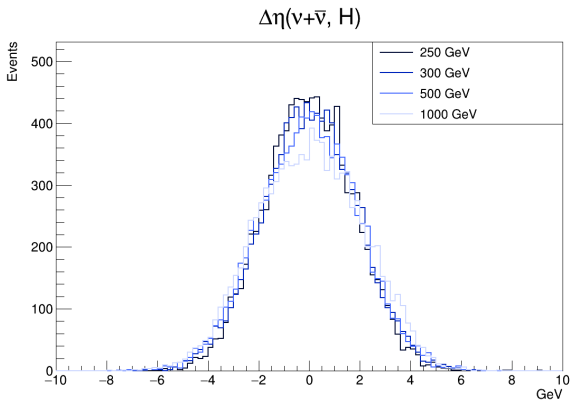

Figure 16: Difference in pseudorapidity between the neutrino–antineutrino system and the Higgs boson.

This existing asymmetry between the neutrino and antineutrino is further illustrated by the distribution of $\Delta\eta =$

$\eta_{\nu\bar{\nu}} - \eta_H$ showed in figure 16, which compares the pseudo-rapidity of the neutrino–antineutrino system to that of the Higgs boson. As the energy increases, the peak of this distribution, initially centred around zero, shifts progressively towards positive values and becomes less pronounced. The shift also suggests an increasingly forward boost of the Higgs boson relative to the neutrino system, potentially influenced by the enhanced role of vector boson fusion at higher energies.

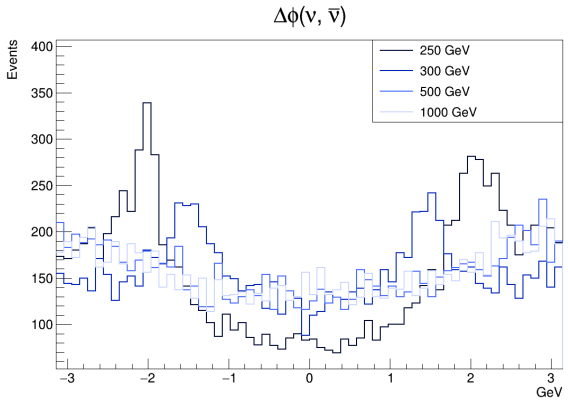

Figure 17: The azimuthal angular separation between the neutrino and the antineutrino.

In the azimuthal angle (ϕ) plane, no clear asymmetry is observed between the neutrino and the antineutrino. The distribution of $\Delta\phi = \phi_\nu - \phi_{\bar{\nu}}$ represented at fidure 17 appears consistent with a symmetric emission pattern across the energy range considered. The slight deviation seen at $\sqrt{s} = 250$ GeV is not present at higher energies and after performing a simulation of this process with 50,000 events instead of 10,000, we concluded that the previously observed discrepancy was not present in the larger sample and is therefore better interpreted as a statistical fluctuation rather than a physical phenomenon..

Additional $\Delta\eta$ and $\Delta\phi$ distributions were also produced for other particles. However, no significant features or deviations from the expected behaviour were observed in those cases as we can see in figure 18.

D. Expected Number of Events

This section presents the expected number of events for the simulated processes, calculated from the production cross-sections and an assumed integrated luminosity. The effect of including the Higgs boson decay into a $b\bar{b}$ pair is also considered. The expected number of events was calculated using the formula:

$$N = \sigma \times \mathrm{BR} \times \int L dt$$

where:

- σ denotes the production cross-section in picobarns (pb),
- $\int L\,dt = 2000\ \mathrm{fb}^{-1} = 2 \times 10^6\ \mathrm{pb}^{-1}$ is the integrated luminosity assumed for all simulations,
- BR represents the branching ratio of the Higgs boson decay channel under consideration, specifically $\mathrm{BR}(H \to b\bar{b}) = 0.58$.

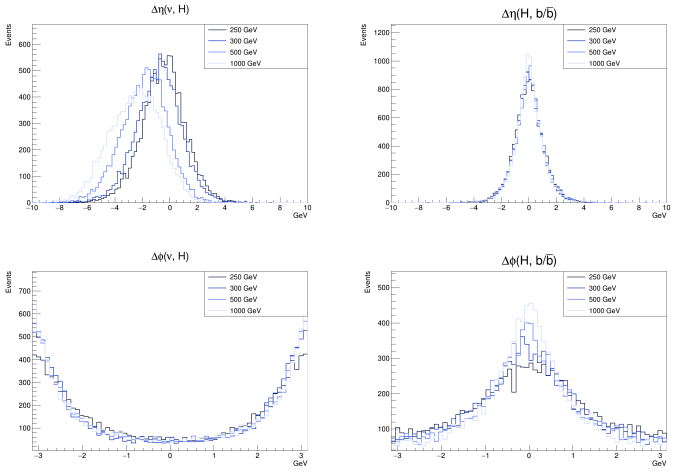

Figure 18: Distributions of $\Delta\eta$ (top row) and $\Delta\phi$ (bottom row) between different particle pairs in the process $e^+e^- \to \nu\bar{\nu}H$, with the Higgs boson decaying into a $b\bar{b}$ pair. The left column shows the separation between the neutrino system and the Higgs boson, while the right column shows the separation between the Higgs boson and the $b\bar{b}$ system.

The result N is dimensionless and represents the expected number of events.

With the cross sections generated in all simulations we proceeded with the calculations having obtained the following values shown in the tables.

Process: $e^+e^- \to \nu\bar{\nu}H$ with Higgs Decay ($H \to b\bar{b}$)

$\sqrt{s}$ [GeV]	σ [pb]	Expected Events N
250	0.01940 ± 0.00005	22481 ± 61
300	0.02329 ± 0.00006	27092 ± 66
500	0.06412 ± 0.00011	74370 ± 124
1000	0.17478 ± 0.00030	203942 ± 351

Table I: Cross-sections and expected number of events for the process $e^+e^- \to \nu\bar{\nu}H$ with explicit Higgs decay.

The results for the process $e^+e^- \to \nu\bar{\nu}H$ with explicit Higgs decay show a clear increase in both the cross-section and the expected number of events as the energy rises from 250 to 1000 GeV. This fact reflects the growing dominance of the vector boson fusion mechanism at higher energies, which enhances the production rate of the Higgs boson.

The relatively small uncertainties on the predicted event yields ensure that this growth is statistically robust. These results confirm that, even when the Higgs decay is fully simulated at the matrix-element level, the $\nu\bar{\nu}H$ channel remains particularly promising for high-energy e^+e^- colliders aiming to study the Higgs boson in clean environments.

E. Probing Higgs Couplings Beyond the SM

To investigate the sensitivity of future lepton colliders to deviations from the Standard Model (SM) in the electroweak Higgs sector, we focus on the process

$$e^+e^- \to \nu\bar{\nu}H, \quad \text{with } H \to b\bar{b},$$

under the presence of beyond the standard model physics interactions that manifest themselves as a dimension-six operator that modifies the HWW vertex. This analysis uses the `SMEFTsim_U35_MwScheme_UFO` model implemented in `MadGraph5_aMC@NLO`, which allows the inclusion of CP-even and CP-odd effective couplings. In particular, we investigate the impact of the CP-even parameter c_{HW}, which modifies the structure of the Higgs coupling to W bosons without violating CP symmetry, and the CP-odd parameter $c_{H\tilde{W}}$, which introduces CP-violating effects in the same vertex. These couplings lead to distinct modifications in the production and decay kinematics of the Higgs boson.

Simulations were carried out for seven values of the Wilson coefficient: the case of the Standard Model value 0, and six non-zero cases: 0.3, 0.6, and 1.0 and this same numbers but in negative, -0.3, -0.6 and -1.0, each of these values was applied simultaneously to the CP-even and CP-odd couplings c_{HW} and $c_{H\tilde{W}}$. The higher values are chosen to be near the upper bounds allowed by current experimental constraints, in order to maximise the visibility of new physics effects. The analysis was restricted to energies of 300 GeV and 1000 GeV, as these represent key benchmark energies proposed for future colliders such as the FCC-ee and the ILC. These choices also reduce visual clutter in the plots by avoiding an excessive number of overlaid curves, thereby improving readability.

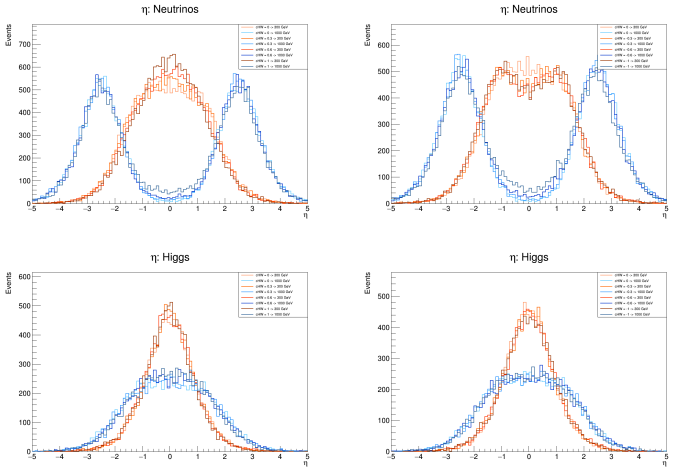

Figure 19: Pseudorapidity (η) distributions of the neutrinos (top), Higgs boson (middle), and $b\bar{b}$ system (bottom) in $e^+e^- \to \nu\bar{\nu}H$, with $H \to b\bar{b}$. Left: CP-even new physics ($c_{HW} > 0$); right: CP-odd ($c_{H\tilde{W}} > 0$).

The pseudorapidity distributions shown in figure 19 reveal no major distortions due to the presence of new physics, either CP-even or CP-odd. However, a mild effect can be observed in some of the plots: as the values of c_{HW} increase (right) or decrease in de case of the negative values (left), the height of the distribution peaks either increases or decreases slightly, depending on the particle and energy configuration. This reflects small shifts in the angular spread of the final-state particles, but the overall shapes remain qualitatively similar to the Standard Model case.

This pattern is also reflected in the transverse and total momentum distributions. While the overall shapes remain largely consistent with Standard Model predictions, slight variations in the peak regions can be seen as the values of c_{HW} increase (right) or decrease in de case of the negative values (left). In particular, some distributions exhibit marginal enhancements or suppressions in the number of events at specific momentum ranges, suggesting a mild sensitivity of these observables to the presence of new physics, especially at higher energies.

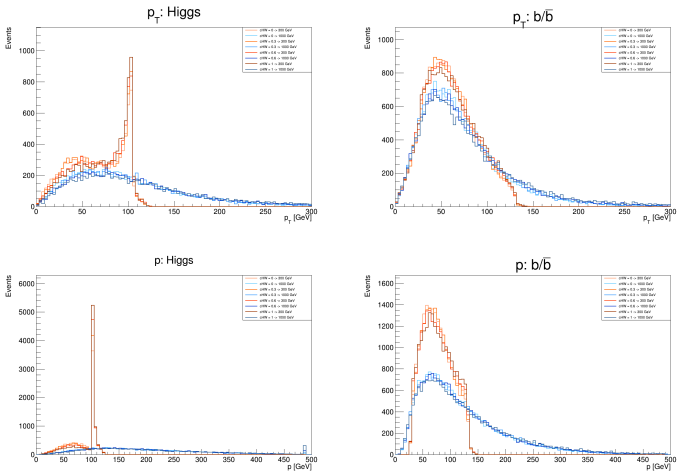

Figure 20: Transverse (p_T, top) and total (p, bottom) momentum distributions of the Higgs boson (left) and $b\bar{b}$ system (right) in $e^+e^- \to \nu\bar{\nu}H$, with $H \to b\bar{b}$, for various values of the CP-even coupling c_{HW}.

As can be seen in the selected plots of figure 21, the transverse momentum (p_T, top row) and total momentum (p, bottom row) distributions of the Higgs boson (left column) and the $b\bar{b}$ system (right column) exhibit distinct behaviours as the CP-even coupling c_{HW} varies.

The Higgs transverse momentum and total momentum distributions exhibit a reduction in peak height, suggesting a suppression of events with characteristic Higgs kinematics. In contrast, the transverse and total momentum distributions of the $b\bar{b}$ system show enhanced peaks, particularly near 300 GeV, indicating that the presence of the CP-even coupling c_{HW} amplifies the kinematic recoil of the decay products. These effects highlight the sensitivity of both production and decay observables to deviations from the Standard Model.

These results demonstrate that the kinematic distributions of the final-state particles in the process $e^+e^- \to \nu\bar{\nu}H$, $H \to b\bar{b}$ are sensitive to new CP-even interactions encoded by the effective coupling c_{HW}. As this coefficient increases, the neutrino system becomes more boosted, and the Higgs boson recoils with higher transverse and total momentum.

This conclusion is further supported by the $\Delta\eta$ and $\Delta\phi$ distributions shown in figure 21, where the impact of varying c_{HW} is again evident. Compared to the Standard Model case, the presence of non-zero CP-even or CP-odd couplings leads to noticeable modifications in the shape and peak structure of these angular correlations between the neutrinos. These variations reinforce the sensitivity of angular observables to new physics effects in the $e^+e^- \to \nu\bar{\nu}H$ process.

With this analysis we open the possibility for future studies including CP-odd operators such as $\tilde{c}_{HW}$, which would allow tests of CP violation in the Higgs sector and may contribute to our understanding of the matter–antimatter asym-

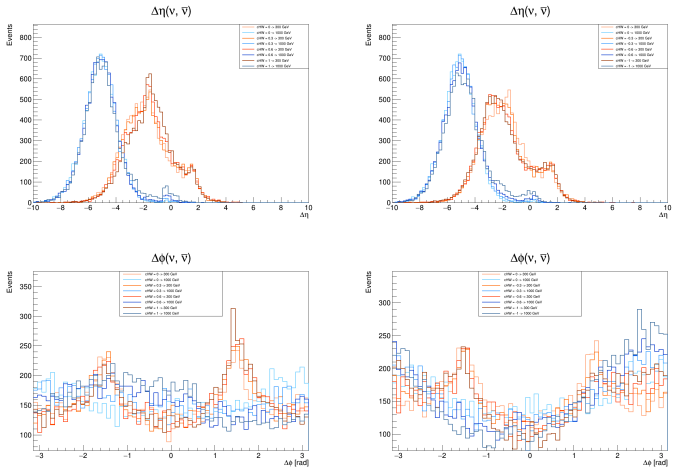

Figure 21: Distributions of $\Delta\eta$ (top) and $\Delta\phi$ (bottom) between neutrinos in $e^+e^- \to \nu\bar{\nu}H$, with $H \to b\bar{b}$. Left: $c_{HW} > 0$; right: $c_{HW} < 0$.

metry in the Universe.

VIII. CONCLUSION

This comprehensive simulation study contributes to our understanding of the physics potential of future electron–positron colliders, such as the FCC-ee and the ILC, by evaluating their sensitivity to deviations in the Higgs boson's couplings. Two production channels were studied: $e^+e^- \to \nu\bar{\nu}H$ and $e^+e^- \to ZH$, focusing on the decay $H \to b\bar{b}$. The $\nu\bar{\nu}H$ channel exhibits a marked increase in cross-section and event yield from 250 GeV to 1 TeV, yielding over 200,000 expected $H \to b\bar{b}$ decays at an integrated luminosity of 2000 fb^{-1}, underlining the potential of high-energy colliders for precise Higgs measurements.

The detailed kinematic analyses of pseudorapidity (η), transverse momentum (p_T), and total momentum (p) distributions reveal characteristic features of the production mechanisms and final-state configurations. The double-peaked η distributions in $\nu\bar{\nu}H$ production arise from neutrino and antineutrino being combined in the same histogram, with symmetric contributions due to their opposite directions. In contrast, the b-jets from $H \to b\bar{b}$ remain mainly central. Momentum distributions evolve with increasing $\sqrt{s}$, while angular correlations ($\Delta\eta$, $\Delta\phi$) further characterise the event topology, especially the energy-dependent recoil of the $\nu\bar{\nu}$ system.

Furthermore, the inclusion of the dimension-six CP-even operator c_{HW} and $c_{H\tilde{W}}$ within the SMEFT framework induces small deviation in the distortions of both momentum and angular distributions, particularly at higher energies. Modifications in the peak structures of p_T and p spectra as well as subtle reshaping in $\Delta\eta$ and $\Delta\phi$ demonstrate that it will be difficult to disentangle beyond the standard model effects of this nature.

Studies such as the one presented here contribute to our understanding of the physics potential of future facilities. The results obtained reinforce the importance of precision measurements in advancing our knowledge of the Higgs boson and its role in electroweak symmetry breaking. While the Standard Model remains consistent with current experimental data, the possibility of small deviations, detectable only through high-precision experiments, remains open. The ability of future colliders such as the FCC-ee and ILC to constrain or reveal such effects will be crucial for guiding theoretical progress, exposing the limitations of the current framework, and potentially uncovering new phenomena underlying the fundamental structure of the universe.

REFERENCES

[1] CERN, "The standard model." https://home.cern/science/physics/standard-model, n.d. Accessed: 2025-05-16.

[2] G. P. Salam, L.-T. Wang, and G. Zanderighi, "The higgs boson turns ten," *Nature*, vol. 607, pp. 41–47, 2022.

[3] M. Thomson, *Modern Particle Physics*. Cambridge: Cambridge University Press, 2013.

[4] ATLAS Collaboration, "The standard model and beyond." https://opendata.atlas.cern/docs/documentation/introduction/SM_and_beyond, n.d. Accessed: 2025-05-17.

[5] A. A. et al. (FCC Collaboration), "Fcc-ee: The lepton collider – future circular collider conceptual design report," *Eur. Phys. J. ST*, vol. 228, pp. 261–623, 2019.

[6] J. Alwall, R. Frederix, S. Frixione, V. Hirschi, F. Maltoni, O. Mattelaer, H.-S. Shao, T. Stelzer, P. Torrielli, and M. Zaro, "The automated computation of tree-level and next-to-leading order differential cross sections, and their matching to parton shower simulations," *JHEP*, vol. 07, p. 079, 2014.

[7] M. Iwamoto, "Lecture b: Monte carlo simulation," 2024. Accessed: 2025-02-08.

[8] S. Funatsu, H. Hatanaka, Y. Hosotani, and Y. Orikasa, "Single higgs boson production at electron-positron colliders in gauge-higgs unification," *arXiv preprint arXiv:2303.02584*, 2023.

[9] CERN, "Future circular collider (fcc)." https://fcc.web.cern.ch/. Accessed: 2025-05-8.

[10] FCC Collaboration, "Future circular collider conceptual design reports." https://fcc-cdr.web.cern.ch, 2019. Accessed: 2025-05-18.

[11] LIP, "High energy physics group – fcc project." https://www.lip.pt/?section=research&page=research-group-details&details=project&projectid=97&line=LH. Accessed: 2025-05-20.

[12] LIP, "Lip contributes to the future circular collider project." https://www.lip.pt/?section=press&page=news-details&id=706&ref=homepage. Accessed: 2025-05-20.

[13] T. N. et al., "Status of the international linear collider." Submitted on behalf of the ICFA ILC International Development Team, April 2025. Available for the European Strategy Update.